

# Statistically induced topological phase transitions in one-dimensional superlattice anyon-Hubbard model

Zheng-Wei Zuo,<sup>1</sup> Guo-Ling Li,<sup>1</sup> and Liben Li<sup>1</sup>

<sup>1</sup>*School of Physics and Engineering, and Henan Key Laboratory of Photoelectric Energy Storage Materials and Applications, Henan University of Science and Technology, Luoyang 471003, China*

(Dated: October 9, 2018)

We theoretically investigate topological properties of the one-dimensional superlattice anyon-Hubbard model, which can be mapped to a superlattice bose-Hubbard model with an occupation-dependent phase factor by fractional Jordan-Wigner transformation. The topological anyon-Mott insulator is identified by topological invariant and edge modes using exact diagonalization and density-matrix renormalization-group algorithm. When only the statistical angle is varied and all other parameters are fixed, a statistically induced topological phase transition can be realized, which provides new insights into the topological phase transitions. What's more, we give an explanation of the statistically induced topological phase transition. The topological anyon-Mott phases can also appear in a variety of superlattice anyon-Hubbard models.

PACS numbers: 71.10.Fd, 71.10.Hf, 73.90.+f, 64.60.Ej

## I. INTRODUCTION

Recently, one-dimensional (1D) topological quantum systems have attracted increasing attentions<sup>1-7</sup>. According to their symmetries, an exhaustive classification of all topological phases of noninteracting fermions has been proposed in Refs.1,2. The Su-Shrieffer-Heeger (SSH) model<sup>8</sup>, The Aubry-André-Harper (AAH) model<sup>9,10</sup>, and the Kitaev chain<sup>11</sup> are three prototypes of 1D noninteracting topological systems in this classification. However, in the presence of strong interactions, the free classification in one-dimensional is radically modified, which breaks down from  $Z$  to  $Z8$ , i.e., there are only eight distinct survived phases<sup>3</sup>. So far, many different analytical and numerical methods such as bosonization technique<sup>12,13</sup>, group cohomology<sup>6</sup>, exact diagonalization<sup>14,15</sup>, and the density matrix renormalization group (DMRG) algorithm have been used to study the 1D topological interacting systems, including Luttinger liquid systems<sup>16-20</sup>, interacting Floquet systems<sup>21-24</sup>, fermion-Hubbard systems<sup>25-27</sup>, and bose-Hubbard systems<sup>28-33</sup>.

The classification of elementary particles as bosons and fermions is crucial to the understanding of a variety of physical systems. However, in low dimensions, particles with others kinds of quantum statistics, anyons, are possible. Because of a wide range of unexpected properties, anyons play a more and more important role in studies of topological order phases of matter<sup>34,35</sup> and topological quantum computation<sup>36</sup>. The 1D anyons systems have exotic and complicated physics properties such as anyonic Bloch oscillations<sup>37</sup>, asymmetric momentum distributions<sup>38,39</sup>, and statistically induced quantum phase transitions<sup>40</sup>. Particularly interesting is the recent proposal of the 1D anyon-Hubbard model<sup>39-49</sup> in optical lattice. Various experimental realizations of anyon-Hubbard model have been proposed<sup>40,41,43,44</sup>, from Raman-assisted tunnel-

ing scheme to lattice shaking-induced resonant tunneling against potential offsets scheme. One of the great advantages of these schemes is the experimental possibility to tune all parameters at will. Theoretical and numerical studies show that the anyon-Hubbard model has a rich physics. Besides the Mott insulator and superfluids, the pair superfluids, dimer phases, and exotic partially paired phase are found<sup>43</sup>. In addition, the symmetry protected topological anyon-Haldane phase emerges from the extended anyon-Hubbard model<sup>47</sup>. Now, the anyon-Hubbard model receives a continuous and extensive interest.

As we know, the superlattice potential<sup>9,10</sup> and electron interaction<sup>3,28,29</sup> can induce the topological phase transition. The interplay of the anyonic statistics, superlattice potential, and interaction may exhibits a rich physics of quantum matter. In this paper, we explore the nontrivial topological properties of 1D anyon-Hubbard model with superlattice potential by exact diagonalization<sup>14,15</sup> and DMRG algorithm<sup>50-52</sup>. The paper is organized as follows. Firstly, we study the topological properties of the Mott insulator phase of superlattice anyon-Hubbard model at strong interaction strength, the topological anyon-Mott insulator is demonstrated by topological invariant and edge modes. Next, we consider the effect of statistical angle on the physical properties of the superlattice anyon-Hubbard model. A statistically induced topological phase transition occurs when the statistical angle increases and other parameters are fixed. In addition, we show the topological phase transition also appears in the off-diagonal superlattice anyon-Hubbard model. Finally, a summary is given.

## II. MODEL AND RESULT

Here, we briefly introduce the 1D superlattice anyon-Hubbard model

## A. Topological Anyon-Mott Insulator

$$H^a = -J \sum_j^{L-1} \left( a_j^\dagger a_{j+1} + h.c. \right) + \sum_j^L \left[ \frac{U}{2} n_j (n_j - 1) + V_j n_j \right] \quad (1)$$

where  $J$  is the hopping strength,  $U$  the on-site two-body interaction energy.  $V_j = V \cos(2\pi\alpha j + \delta)$  stands for a periodic superlattice potential with  $V$  being the modulation amplitude, and  $\delta$  being an arbitrary phase. We consider a commensurate superlattice potential  $V_j$  with modulation period  $\alpha = p/q$  ( $p, q$  are integers) being a rational number. Here,  $a_j^\dagger$  ( $a_j$ ) is the creation (annihilation) operator of anyon on site  $j$ ,  $n_j = a_j^\dagger a_j$  is the number operator. These anyons satisfy the generalized commutation relations

$$a_j a_k^\dagger - e^{-\theta \text{sgn}(j-k)} a_k^\dagger a_j = \delta_{kj}, a_j a_k = e^{\theta \text{sgn}(j-k)} a_k a_j \quad (2)$$

where  $\theta$  denotes the statistical phase, and the sign function  $\text{sgn}(j-k) = (j-k)/|j-k|$  for  $j \neq k$ , and  $\text{sgn}(j-k) = 0$  for  $j = k$ , respectively.

By fractional Jordan-Wigner transformation  $a_j = b_j \exp\left(i\theta \sum_{i=1}^{j-1} n_i\right)$ , the superlattice anyon-Hubbard Hamiltonian can be rewritten as a superlattice Bose-Hubbard model with an occupation-dependent phase factor

$$H^b = -J \sum_j^{L-1} \left( b_j^\dagger b_{j+1} e^{i\theta n_j} + h.c. \right) + \sum_j^L \left[ \frac{U}{2} n_j (n_j - 1) + V_j n_j \right] \quad (3)$$

where  $b_j^\dagger$  is a boson creation operator. Due to the occupation-dependent hopping, the reflection parity symmetry is broken. So, we map the superlattice anyon-Hubbard model to an occupation-dependent hopping superlattice boson-Hubbard model. The Hilbert space of anyons can be constructed from that of bosons. For convenience, we take  $J = 1$  as the unit of energy and choose  $\alpha = 1/3$ .

As shown in Ref.40, owing to the unitarity of anyon-boson mapping, the two models are isospectral and they share the same energy gaps and phase diagrams. For the statistical phase  $\theta = 0$ , we can see that the superlattice anyon-Hubbard model reduces to the superlattice boson-Hubbard model<sup>28</sup>. The ground-state phase diagram of superlattice boson-Hubbard model is well-studied<sup>27,28,30-32</sup>. For the anyon case, we hope the interplay of anyonic statistics and interaction lead to a rich physics of quantum phases. Without periodic superlattice potential, the anyon-Hubbard model with repulsive interactions has been observed that Mott insulator and superfluid phases characterized the phase diagram<sup>39-41,43-46</sup>. Here, we focus on the topological properties of the Mott insulator phase.

As we know, the superlattice anyon-Hubbard model is in superfluid phases for a small  $U$ . As the interaction  $U$  increases, the system transits into Mott phase. Now, we investigate the topological properties of the Mott insulator phase using DMRG algorithm and exact diagonalization.

Firstly, we tune the parameters of Hamiltonian to obtain the Mott state, which can be characterized by the energy gap (particle-hole excitation)<sup>15,45</sup>, which is difference between quasiparticle and quasihole energy spectra. The quasiparticle and quasihole energy spectra can be defined as

$$\mu_p(N) = E_{N+1} - E_N \quad (4)$$

$$\mu_h(N) = E_N - E_{N-1} \quad (5)$$

where  $E_N$  is the ground-state energy of the system with  $N$  anyons. So, the energy gap  $\Delta\mu$  can be obtained via

$$\Delta\mu = \mu_p(N) - \mu_h(N) = E_{N+1} + E_{N-1} - 2E_N \quad (6)$$

At the thermodynamic limit, the gap  $\Delta\mu$  is finite and zero in Mott and superfluid phases, respectively. We start considering the superlattice anyon-Hubbard model with the number of anyons  $N$  and the lattice sites  $L$ . The filling factor is defined as  $\nu = N/L = m\alpha$  with  $m$  being an integer. Here, we set  $\alpha = \nu = 1/3$ ,  $m = 1$ ,  $U = 10$ ,  $V = 10$ ,  $\delta = 2\pi/3$ . Using the DMRG algorithm based on the ITensor library<sup>53</sup>, we numerically get the system size dependence of the gap  $\Delta\mu$  of anyon in anyon-Hubbard superlattice with statistical angle  $\theta = 0, \pi/5, 2\pi/5, 3\pi/5, 4\pi/5, \pi$  with period boundary condition (PBC), which is shown in Fig. 1. The maximal boson number per site in DMRG is constrained to be four.

From Fig.1, we can see that the gap  $\Delta\mu$  remain finite values for  $\theta = 0, \pi/5, 2\pi/5, 3\pi/5, 4\pi/5, \pi$  at the thermodynamic limit. These results suggest that the ground states correspond to Mott insulator phases for any statistical angle  $\theta$ . In the following sections, we mainly focus on the topological feature of superlattice anyon-Hubbard model for  $0 \leq \theta \leq \pi$ .

The topological property of these Mott states can be demonstrated by the Chern number for many-body interacting system<sup>54</sup>. First, let us introduce the twisted boundary condition  $|\psi(j+L, \delta, \phi)\rangle = e^{i\phi} |\psi(j, \delta, \phi)\rangle$  where  $j$  denotes an arbitrary site,  $\alpha$  is the twist angle and takes values from 0 to  $2\pi$ . Then, the Chern number  $C$  as a topological invariant can be calculated by the following formula

$$C = \frac{1}{2\pi} \int_0^{2\pi} \int_0^{2\pi} F(\delta, \phi) d\delta d\phi \quad (7)$$

where  $F(\delta, \phi) = \text{Im} \left( \left\langle \frac{\partial \psi}{\partial \phi} \middle| \frac{\partial \psi}{\partial \delta} \right\rangle - \left\langle \frac{\partial \psi}{\partial \delta} \middle| \frac{\partial \psi}{\partial \phi} \right\rangle \right)$  is the Berry curvature and  $\psi$  many-body ground-state wave

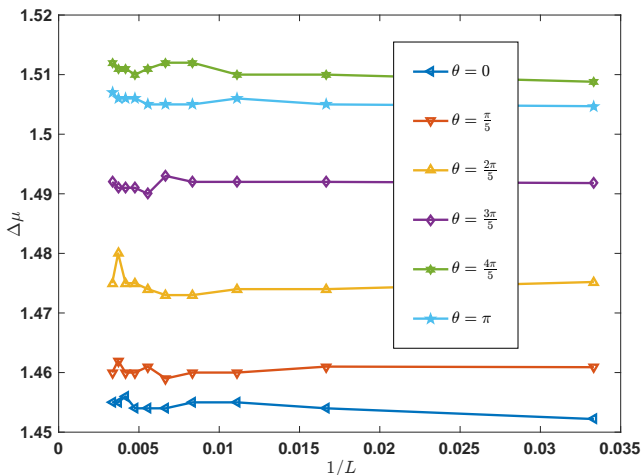


FIG. 1: (Color online) System size dependence of the gap  $\Delta\mu$  of anyon in anyon-Hubbard superlattice with statistical angle  $\theta = 0, \pi/5, 2\pi/5, 3\pi/5, 4\pi/5, \pi$ ,  $U = 10, V = 10, \delta = 2\pi/3, \alpha = \nu = 1/3$ .

function of the system. The Chern number can be interpreted as numbers of anyon charge pumped in one cycle of  $\delta$  for the superlattice anyon-Hubbard model. We numerically calculate the Chern numbers of the ground states. By using the exact diagonalization and the discrete set of values of  $(\delta, \phi)$ , we calculate the Chern number  $C^{55}$  with system size  $L=15$ . We find that the Chern number  $C = 1$ . These calculations demonstrate that these Mott states are topological. The topological properties of the Mott states with other statistical angles can be analyzed similarly. We refer to these topological Mott states as *topological anyon-Mott insulator*. For the statistical angle  $\theta = 0$ , the results are consistent with those calculations for superlattice Bose-Hubbard model and the topological Bose-Mott insulator is obtained<sup>28</sup>.

According to the bulk-edge correspondence, there are edge modes (localized modes) in topological interacting systems characterized by the quasiparticle density distribution<sup>27–32</sup>. The density distribution of the quasiparticle can be defined as

$$\Delta n_j = \langle \psi_{n+1}^g | n_j | \psi_{n+1}^g \rangle - \langle \psi_n^g | n_j | \psi_n^g \rangle \quad (8)$$

where  $\psi_n^g$  denotes the ground state wave function of the system with  $n$  bosonic atoms for open boundary condition (OBC), the quasihole case has similar formula. The results with different statistical angles  $\theta$  for  $N = 30, L = 90$  using DMRG algorithm are shown in Fig. 2. Such edge modes which mainly distribute near one end site of the chain can be seen in Fig. 2, which are consistent with the topological invariant Chern numbers.

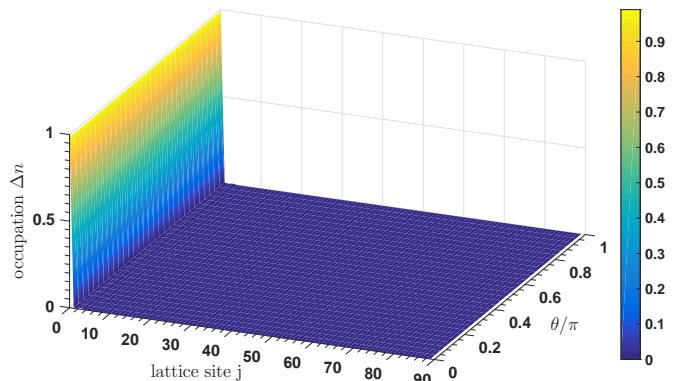


FIG. 2: (Color online) The density distribution of the quasiparticle along the lattice sites at  $N = 30, L = 90$ . The other parameters are the same as those for Fig.1.

## B. Statistically Induced Topological Phase Transition

Now, we consider the effect of statistical angle on the physics properties of the superlattice anyon-Hubbard model. Here, we take the parameters  $U = 2, V = 1, \delta = 2\pi/3, \alpha = \nu = 1/3$  as an example. To begin with, the evolution of the gap  $\Delta\mu$  versus the inverse of the lattice length appear in Fig. 3. At the thermodynamic limit, the value of the gap  $\Delta\mu$  is zero and the ground state is superfluid at  $\theta = 0$ . However, at  $\theta = 4\pi/5, \pi$ , the gap  $\Delta\mu$  remain finite value and the ground states are in Mott state. This figure suggests that the system transits from superfluid into Mott phase when the statistical angle increases, so the phase transition takes place. Next, we demonstrate that these Mott states are topological.

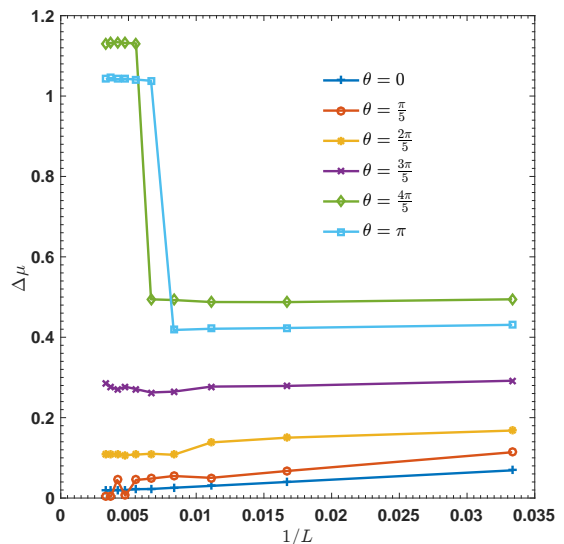


FIG. 3: (Color online) System size dependence of the gap  $\Delta\mu$  of anyon in anyon-Hubbard superlattice with statistical angle  $\theta = 0, \pi/5, 2\pi/5, 3\pi/5, 4\pi/5, \pi$ , and  $U = 2, V = 1, \delta = 2\pi/3, \alpha = \nu = 1/3$ .

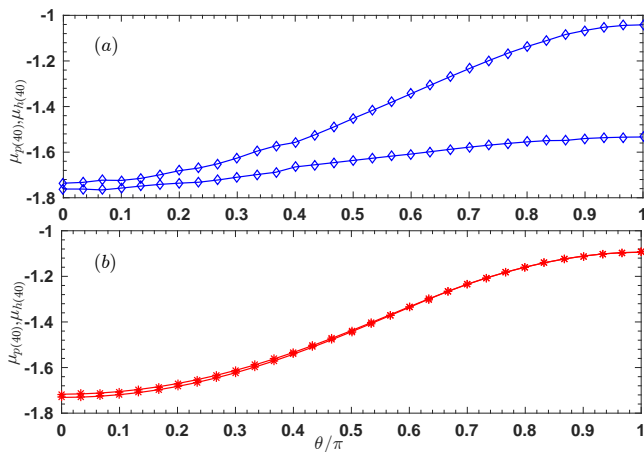


FIG. 4: (Color online) The quasiparticle and quasihole energy spectra versus the statistical angle  $\theta$  for anyon-Hubbard superlattice with  $L = 120$ ,  $U = 2$ ,  $V = 1$ ,  $\delta = 2\pi/3$ ,  $\alpha = \nu = 1/3$ ; (a) Period boundary condition (b) Open boundary condition.

When the system has a nontrivial topological property, there are states in the gap of the quasiparticle energy spectrum as the boundary condition changes from PBC to OBC<sup>56</sup>. Now, the calculations are taken that quasiparticle and quasihole energy spectra versus the statistical angle  $\theta$  with  $L = 120$ ,  $U = 2$ ,  $V = 1$ ,  $\delta = 2\pi/3$ ,  $\alpha = \nu = 1/3$  for (a) PBC and (b) OBC, which are shown in Fig. 4. This figure shows that the gap  $\Delta\mu$  becomes more and more larger for PBC when the statistical angle increases. For large  $\theta$ , the system transits into the Mott phase ( $\Delta\mu=0.492$  for  $\theta = \pi$ ), as shown in Fig. 3. The energies of quasiparticles added or removed (for OBC) appear in the gap (for PBC) when the statistical angle exceeds a critical value. The two in-gap modes have exactly the same values for larger statistical angle. For small  $\theta$ , the system enters into the superfluid phase, as shown in Fig. 3. These two in-gap modes disappear and evolve into the bulk ones. The differences of quasiparticle and quasihole energy spectra are very small for small  $\theta$ . For example, the difference of quasiparticle spectrum for PBC and OBC is 0.0193 and the difference of quasihole spectrum is 0.0308. These values should have a tendency to zero at the thermodynamic limit because of the superfluid regime. These results show that topological phase transition arises when the statistical angle is large. When the statistical angle increases, the topological quantum transition occurs. As we know, one of the weaknesses of the DMRG is that it works poorly with PBC. This stems from the fact that conventional DMRG optimizes over open-boundary matrix product state wave-functions. For the larger size, the accuracy of data maybe drastically lower under PBC. This may be why the data  $\theta = 4\pi/5$  and  $\pi$  show weird behavior in Fig. 3. So, the critical statistical angle of this topological quantum transition should be estimated by the data of DMRG with OBC and Chern number.

To illustrate the topological quantum transition clearly, we calculate quasiparticle energy spectrum with respect to the phase parameter  $\delta$  around the filling factor  $\nu = 1/3$  by way of DMRG algorithm under OBC. In Fig. 5, we show the quasiparticle energy spectrum  $\mu_p(N)$  ( $N = 41, 40, 39$ , and  $38$ ) as a function of the phase parameter  $\delta$  with  $L = 120$ ,  $U = 2$ ,  $V = 1$ , and  $\theta = 0, \pi/5, 2\pi/5, 3\pi/5, 4\pi/5, \pi$ . As illustrated in the figures, there is a quasiparticle finite gap for every  $\theta$  when deviating from filling factor  $\nu = 1/3$  ( $N = 41, 38$ ). For the  $\theta = 3\pi/5, 4\pi/5$ , and  $\pi$ , there exist two branches of quasiparticle modes which cross each other and connect the lower and upper bands of quasiparticle energy spectra as the  $\delta$  varies from 0 to  $2\pi$ . However, for  $\theta = 0, \pi/5$ , and  $2\pi/5$ , the two quasiparticle modes do not connect the lower and upper bands. From the Fig. 5, it is clear that with the increasing statistical angle, a topological quantum transition takes place and the critical statistical angle is around the  $3\pi/5$ .

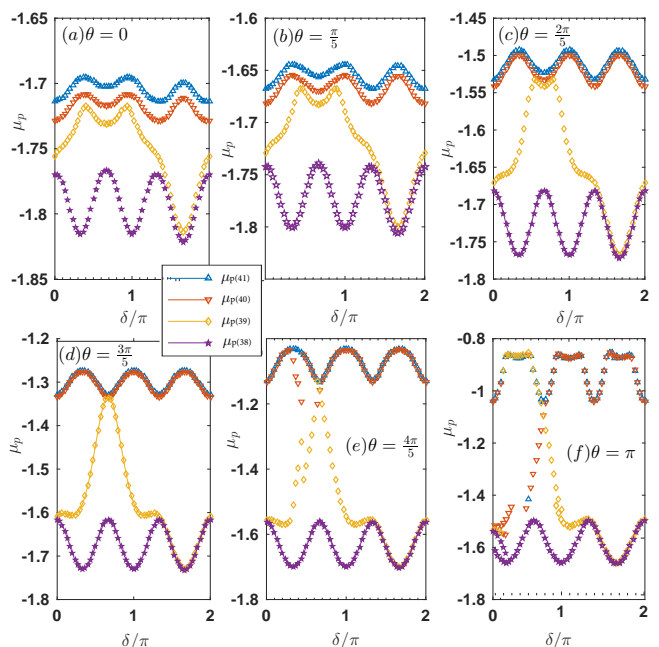


FIG. 5: (Color online) The quasiparticle energy spectrum  $\mu_p(N)$  ( $N = 41, 40, 39$ , and  $38$ ) with respect to phase parameter  $\delta$  for anyon-Hubbard superlattice with  $L = 120$ ,  $U = 2$ ,  $V = 1$ , and  $\theta = 0, \pi/5, 2\pi/5, 3\pi/5, 4\pi/5, \pi$  under OBC.

Next, we verify that these crossing in-gap modes correspond to the end states and calculate the quasiparticle density distribution of these modes, and then compute the system's topological invariants. Here, we set the parameters  $L = 120$ ,  $N = 40$ ,  $U = 2$ ,  $V = 1$ , and  $\delta = 2\pi/3$ . According to Eq. (8), the calculations are straightforward and the result (only quasiparticle case) is shown in Fig. 6. As the statistical angle increases, the density distribution begins to evolve from the bulk to the ends. For  $\theta > 9\pi/10$ , we can see that more than 30% of the quasiparticle modes are localized at the end sites, which

are hallmark of topologically nontrivial phase. The larger statistical angle is, the more probability of quasiparticle are localized at the ends. From Fig. 6, we can see that the critical statistical angle  $\theta_c$  is about  $0.65\pi$ . The numerical results show that there is great probability distribution localized at the end sites when we adjust the phase parameter  $\delta$  and/or periodic superlattice potential  $V$  in topological anyon-Mott phase. Varying  $\delta$  continuously from 0 to  $2\pi$ , one can see that the end states change from one side to the other.

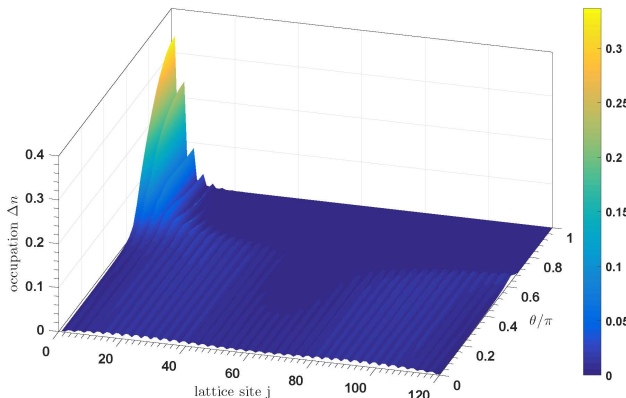


FIG. 6: (Color online) The distribution of the quasiparticle along the lattice sites at  $L = 120, 0 \leq \theta \leq \pi$ . The other parameters are the same as those for Fig.3.

In the following, we calculate the topological invariants for the system with  $\theta = 4\pi/5$  in the Mott regime. The topological property of the bulk Mott state with concrete  $\delta = 2\pi/3$  can be characterized by the Berry phase using the twisted boundary condition defined above. The Berry phase can be defined as

$$\gamma = \oint i \left\langle \psi(\phi) \left| \frac{d}{d\phi} \right| \psi(\phi) \right\rangle \quad (9)$$

We find that the Berry phase  $\gamma = \pi$ , which shows the topological property of the Mott state is nontrivial. In some region of the superfluid (for small  $\theta$ ) phase, Berry phase is still approximately  $\pi$ , because of the finite-size gap. In addition, we can calculate the Chern number of the system with  $\theta = 4\pi/5$  within  $(\delta, \phi)$ -space and find the Chern number is quantized as  $C = 1$ . This topological Mott state is also the topological anyon-Mott insulator state. With fixed  $J, U$ , and  $V$ , this phase transition is only driven by the statistical angle  $\theta$ . Taking into account the above discussion and these numerical results, we refer this phase transition as *statistically induced topological phase transition*. In principle, we can get the phase diagram by calculating the Chern number or Berry phase. Here, we give the phase diagram for the system with  $L = 15, N = 5$ , and  $V = 1$  using the Chern number and the Mott gap between ground and first excited state of the system with  $L = 18, N = 6, V = 1$ , and  $\delta = 2\pi/3$ , which are shown in Fig.7 (a) and (b). From Fig.7 (a), we can see that in some superfluid

region, Chern numbers remain the value of 1 due to the finite-size gap. Although, we cannot obtain the precise phase diagram by the Chern number, the Mott gap can approximately reflect the evolution behaviors of the system by exact diagonalization. For every statistical angle, the Mott gap tends to a saturation value and zero at larger and smaller  $U$ , respectively, which correspond to the Mott and superfluid regions as shown in Fig.7 (b). The larger the statistical angle becomes, the earlier the system enters into the topological anyon-Mott phase. With the statistical angle increasing, the critical value of the superfluid to topological anyon-Mott phase transition becomes smaller and smaller. Thus, for a fixed  $U$  (for example  $U = 2$ ), the system can transfer from the superfluid phase into the topological anyon-Mott phase as the statistical angle increases. In a word, as the value of statistical angle is varied, the statistically induced topological phase transition emerges.

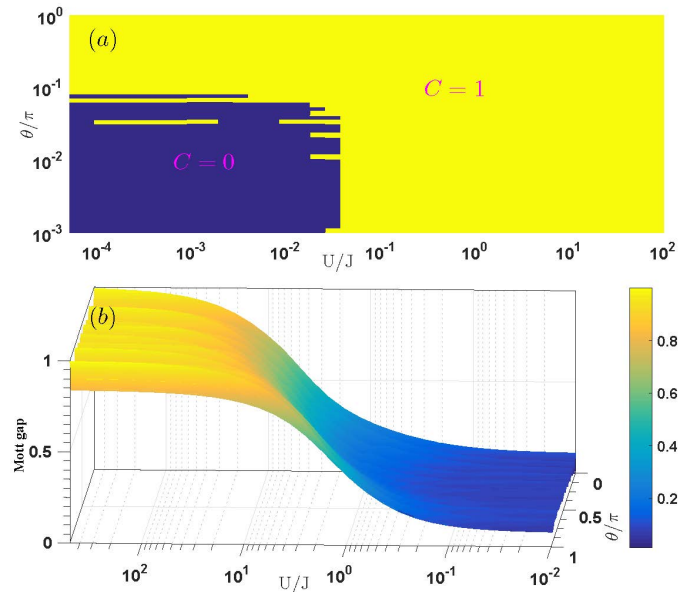


FIG. 7: (Color online) (a) The phase diagram for the system with  $L = 15, N = 5$ , and  $V = 1$ ; (b) The Mott gap of the system with  $L = 18, N = 6, V = 1$  and  $\delta = 2\pi/3$ .

The statistically induced topological phase transition can be understood by the following argument: Using bosonization technique, Greschner and coauthors have shown that the anyonic exchange statistics has qualitatively the same effect as repulsive interaction in anyon-Hubbard with weakly interaction regime<sup>41,43</sup>. The effect of anyonic exchange statistics can be described by a scattering length that describes repulsive interactions. With increasing anyonic angle, the effect scattering length increases which shows that the repulsive interaction becomes bigger. So anyonic exchange statistics and repulsive interaction may have the same effect on phase diagram. The Mott lobes grows as the statistical angle increases, as shown by previous results<sup>40,41,43,45,49</sup>. Thus, we can take the statistical angle as an effective repulsion

interaction parameter. What's more, the occupation-dependent phase factor in Eq. (3) becomes more and more important with increasing  $\theta$ . Because of the incoherent superpositions, nearest neighbor tunneling processes would cancel out in the kinetic Hamiltonian and contribute different values. The increase of statistical angle enhances the destructive interference effect<sup>40</sup>. At the same time, anyons with statistics angle  $\theta = \pi$  are pseudofermions, because they are fermions off-site, while being bosons on-site. For large statistical angle  $\theta \approx \pi$ , the generalized off-site commutation relations of anyons tend to generate a Pauli-exclusion principle. As a result, the particles are more localized and an insulating phase would appear. On the other hand, the bose interaction can induce the topological phase transition in superlattice Bose-Hubbard model. So, the anyonic exchange statistics can also drive the system into topological anyon-Mott insulator states as we shown above.

### C. Off-diagonal Anyon-Hubbard Superlattice

As shown above, anyonic statistics and interaction result in a rather rich physics in diagonal superlattice anyon-Hubbard model. In the following, we discuss other types of superlattice anyon-Hubbard model. Here we consider 1D off-diagonal superlattice anyon-Hubbard model, which can be defined as

$$H^a = - \sum_j^{L-1} (J_j a_j^\dagger a_{j+1} + h.c.) + \sum_j^L \frac{U}{2} n_j (n_j - 1) \quad (10)$$

where  $J_j = [1 + V \cos(2\pi\alpha j + \delta)]$ . According to the above methods, we can also show that this off-diagonal superlattice anyon-Hubbard model exhibits the topological anyon-Mott insulator phase and the statistical angle can induce the topological phase transition. Without loss of generality, hereafter we take the parameters  $\alpha = 1/2$ ,  $\nu = 1/2$ ,  $U = 1$ ,  $V = 0.9$ ,  $\delta = 0$ ,  $L = 120$  as an example. As the anyonic statistical angle increases, the edge modes begin to appear and topological phase transition occurs, as shown by Fig. 8. What's more, we numerically calculate the Berry phase and find  $\gamma = \pi$  in topological anyon-Mott states. In a word, the statistically induced topological phase transition exhibits in diagonal and off-diagonal superlattice anyon-Hubbard models.

### III. CONCLUSION

In summary, we have researched the nontrivial topological properties of the one-dimensional superlattice anyon-Hubbard model. For the strong interaction strength, the topological anyon-Mott insulator is identified by the edge states and topological invariant. The anyonic exchange statistics affects significantly the ground-state properties of the system. When we take statistical angle as a free controllable parameter, the statistically induced

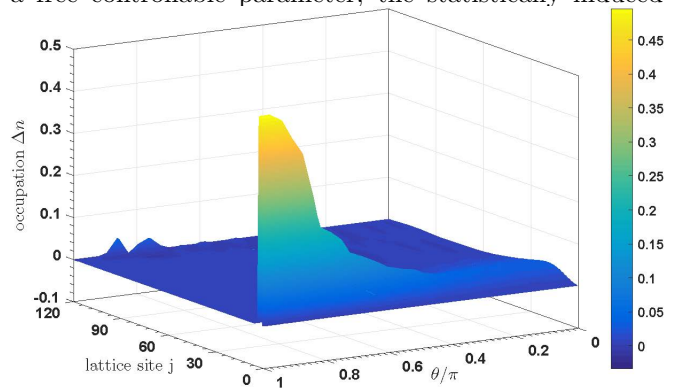


FIG. 8: (Color online) The distribution of the quasiparticle along the lattice sites at  $L = 120$ . The other parameters are  $\alpha = \nu = 1/2$ ,  $U = 1$ ,  $V = 0.9$ ,  $\delta = 0$ .

topological phase transition appears, which provides new insights on the topological phase transitions. Furthermore, we provide an explanation of the statistically induced topological phase transition. In addition, our work may open many directions for the superlattice anyon-Hubbard model. The superlattice anyon-Hubbard model can be generalized to a variety of versions such as incommensurate superlattice potentials, non-Abelian, and non-Hermitian cases. There would be a rich intriguing physics in these models.

*Acknowledgements.*—This work was supported by the National Natural Science Foundation of China under grant numbers 11604081, 11447008 (Z.Z.W.), U1404212 (G.L.L).

<sup>1</sup> A. P. Schnyder, S. Ryu, A. Furusaki, and A. W. W. Ludwig, *Phys. Rev. B* **78**, 195125 (2008).  
<sup>2</sup> A. Kitaev, *AIP Conf. Proc.* **1134**, 22 (2009).  
<sup>3</sup> L. Fidkowski and A. Kitaev, *Phys. Rev. B* **81**, 134509 (2010).  
<sup>4</sup> L. Fidkowski and A. Kitaev, *Phys. Rev. B* **83**, 075103 (2011).  
<sup>5</sup> A. M. Turner, F. Pollmann, and E. Berg, *Phys. Rev. B*

**83**, 075102 (2011).

<sup>6</sup> X. Chen, Z.-C. Gu, and X.-G. Wen, *Phys. Rev. B* **83**, 035107 (2011).

<sup>7</sup> X. Chen, Z.-C. Gu, and X.-G. Wen, *Phys. Rev. B* **84**, 235128 (2011).

<sup>8</sup> W. P. Su, J. R. Schrieffer, and A. J. Heeger, *Phys. Rev. Lett.* **42**, 1698 (1979).

<sup>9</sup> L.-J. Lang, X. Cai, and S. Chen, *Phys. Rev. Lett.* **108**,

- 220401 (2012).
- <sup>10</sup> S. Ganeshan, K. Sun, and S. Das Sarma, *Phys. Rev. Lett.* **110**, 180403 (2013).
  - <sup>11</sup> A. Y. Kitaev, *Phys.-Usp.* **44**, 131 (2001).
  - <sup>12</sup> A. O. Gogolin, A. A. Nersisyan, and A. M. Tsvelik, *Bosonization and strongly correlated systems* (Cambridge Univ. Press, 1998).
  - <sup>13</sup> T. Giamarchi, *Quantum Physics in One Dimension* (Oxford Univ. Press, 2004).
  - <sup>14</sup> J. M. Zhang and R. X. Dong, *Eur. J. Phys.* **31**, 591 (2010).
  - <sup>15</sup> D. Ravents, T. Gra, M. Lewenstein, and B. Juli-Daz, *J. Phys. B: At. Mol. Opt. Phys.* **50**, 113001 (2017).
  - <sup>16</sup> J. Ruhman, E. Berg, and E. Altman, *Phys. Rev. Lett.* **114**, 100401 (2015).
  - <sup>17</sup> A. Keselman and E. Berg, *Phys. Rev. B* **91**, 235309 (2015).
  - <sup>18</sup> N. Kainaris and S. T. Carr, *Phys. Rev. B* **92**, 035139 (2015).
  - <sup>19</sup> A. Montorsi, F. Dolcini, R. C. Iotti, and F. Rossi, *Phys. Rev. B* **95**, 245108 (2017).
  - <sup>20</sup> J. Ruhman, V. Kozii, and L. Fu, *Phys. Rev. Lett.* **118**, 227001 (2017).
  - <sup>21</sup> A. C. Potter, T. Morimoto, and A. Vishwanath, *Phys. Rev. X* **6**, 041001 (2016).
  - <sup>22</sup> C. W. von Keyserlingk and S. L. Sondhi, *Phys. Rev. B* **93**, 245145 (2016).
  - <sup>23</sup> C. W. von Keyserlingk and S. L. Sondhi, *Phys. Rev. B* **93**, 245146 (2016).
  - <sup>24</sup> D. V. Else and C. Nayak, *Phys. Rev. B* **93**, 201103 (2016).
  - <sup>25</sup> Z. Xu, L. Li, and S. Chen, *Phys. Rev. Lett.* **110**, 215301 (2013).
  - <sup>26</sup> Z. Xu and S. Chen, *Phys. Rev. B* **88**, 045110 (2013).
  - <sup>27</sup> H. Guo, *Phys. Rev. A* **92**, 033625 (2015).
  - <sup>28</sup> S.-L. Zhu, Z.-D. Wang, Y.-H. Chan, and L.-M. Duan, *Phys. Rev. Lett.* **110**, 075303 (2013).
  - <sup>29</sup> F. Grusdt, M. Höning, and M. Fleischhauer, *Phys. Rev. Lett.* **110**, 260405 (2013).
  - <sup>30</sup> X. Deng and L. Santos, *Phys. Rev. A* **89**, 033632 (2014).
  - <sup>31</sup> T. Li, H. Guo, S. Chen, and S.-Q. Shen, *Phys. Rev. B* **91**, 134101 (2015).
  - <sup>32</sup> F. Matsuda, M. Tezuka, and N. Kawakami, *J. Phys. Soc. Jpn.* **83**, 083707 (2014).
  - <sup>33</sup> T.-S. Zeng, W. Zhu, and D. N. Sheng, *Phys. Rev. B* **94**, 235139 (2016).
  - <sup>34</sup> A. Stern, *Nature* **464**, 187 (2010).
  - <sup>35</sup> A. Stern, *Annu. Rev. Condens. Matter Phys.* **7**, 349 (2016).
  - <sup>36</sup> C. Nayak, S. H. Simon, A. Stern, M. Freedman, and S. Das Sarma, *Rev. Mod. Phys.* **80**, 1083 (2008).
  - <sup>37</sup> S. Longhi and G. Della Valle, *Phys. Rev. B* **85**, 165144 (2012).
  - <sup>38</sup> Y. Hao, Y. Zhang, and S. Chen, *Phys. Rev. A* **79**, 043633 (2009).
  - <sup>39</sup> G. Tang, S. Eggert, and A. Pelster, *New J. Phys.* **17**, 123016 (2015).
  - <sup>40</sup> T. Keilmann, S. Lanzmich, I. McCulloch, and M. Roncaglia, *Nat. Commun.* **2**, 361 (2011).
  - <sup>41</sup> S. Greschner, G. Sun, D. Poletti, and L. Santos, *Phys. Rev. Lett.* **113**, 215303 (2014).
  - <sup>42</sup> T. M. Wright, M. Rigol, M. J. Davis, and K. V. Kheruntsyan, *Phys. Rev. Lett.* **113**, 050601 (2014).
  - <sup>43</sup> S. Greschner and L. Santos, *Phys. Rev. Lett.* **115**, 053002 (2015).
  - <sup>44</sup> C. Sträter, S. C. L. Srivastava, and A. Eckardt, *Phys. Rev. Lett.* **117**, 205303 (2016).
  - <sup>45</sup> J. Arcila-Forero, R. Franco, and J. Silva-Valencia, *Phys. Rev. A* **94**, 013611 (2016).
  - <sup>46</sup> L. Cardarelli, S. Greschner, and L. Santos, *Phys. Rev. A* **94**, 023615 (2016).
  - <sup>47</sup> F. Lange, S. Ejima, and H. Fehske, *Phys. Rev. Lett.* **118**, 120401 (2017).
  - <sup>48</sup> F. Lange, S. Ejima, and H. Fehske, *Phys. Rev. A* **95**, 063621 (2017).
  - <sup>49</sup> W. Zhang, S. Greschner, E. Fan, T. C. Scott, and Y. Zhang, *Phys. Rev. A* **95**, 053614 (2017).
  - <sup>50</sup> S. R. White, *Phys. Rev. Lett.* **69**, 2863 (1992).
  - <sup>51</sup> U. Schollwöck, *Rev. Mod. Phys.* **77**, 259 (2005).
  - <sup>52</sup> U. Schollwöck, *Annals of Physics* **326**, 96 (2011).
  - <sup>53</sup> *ITensor Library*.
  - <sup>54</sup> Q. Niu, D. J. Thouless, and Y.-S. Wu, *Phys. Rev. B* **31**, 3372 (1985).
  - <sup>55</sup> T. Fukui, Y. Hatsugai, and H. Suzuki, *J. Phys. Soc. Jpn.* **74**, 1674 (2005).
  - <sup>56</sup> H. Guo and S.-Q. Shen, *Phys. Rev. B* **84**, 195107 (2011).